

# Fair Beam Synthesis and Suppression via Transmissive Reconfigurable Intelligent Surfaces

Rujing Xiong<sup>1</sup>, Jialong Lu<sup>1</sup>, Ke Yin<sup>2</sup>, Tiebin Mi<sup>1</sup>, Robert Caiming Qiu<sup>1</sup>

<sup>1</sup> School of Electronic Information and Communications, Huazhong University of Science and Technology

<sup>2</sup> Center for Mathematical Sciences, School of Mathematics and Statistics, Huazhong University of Science and Technology  
Wuhan 430074, China

Email: {rujing, jialong, kyin, mitiebin, caiming}@hust.edu.cn

*Abstract*—Existing phase optimization methods in reconfigurable intelligent surfaces (RISs) face significant challenges in achieving flexible beam synthesis, especially for directional beam suppression. This paper introduces a Max-min criterion incorporating non-linear constraints, utilizing optimization techniques to enable multi-beam enhancement and suppression via transmissive RISs. A realistic model grounded in geometrical optics is first presented to characterize the input/output behavior of transmissive RIS, effectively linking explicit beam-forming operations with practical implementation. Subsequently, a highly efficient bisection-based algorithm for constrained Max-min optimization involving quadratic forms is developed, utilizing an auxiliary variable and Moreau envelope to iteratively reach the optimal solution. This approach demonstrates excellent extensibility and is applicable to a wide range of constrained Max-min problems. Numerical simulations validate the proposed methods, confirming that the framework enables beam enhancement or suppression at designated spatial positions.

*Index Terms*—Transmissive RIS, fair beam synthesis, beam suppression, Max-min optimization, interference elimination

## I. INTRODUCTION

RECONFIGURABLE intelligent surface (RIS) is anticipated to be a pivotal technology for future 6G communications networks due to its great capability to reconfigure and optimize wireless propagation environments [1]. Despite RIS has been demonstrated to enhance system performance in various wireless networks, current implementations predominantly rely on reflective designs, which introduces certain limitations and results in undesirable coverage gaps in practical applications [2]. Specifically, reflective RIS requires both the base station (BS) and the user equipment (UE) to be positioned on the same side of the RIS, imposing additional geographical constraints on the physical topology [3]. For instance, reflective RIS encounters difficulties in facilitating communication between a transmitter outside a vehicle and a receiver inside it, as well as in establishing communication links between indoor and outdoor environments through walls or windows.

To tackle these limitations, the transmissive RIS technique is garnering increasing attention [4], [5]. transmissive RIS allows signals to transmit through itself to form directional beams. Similar to reflective RISs, transmissive RISs can be utilized to

establish extra refractive communication links between the BS and UE. Additionally, due to the absence of physical topology constraints, transmissive RIS is increasingly utilized to design novel transmitter architectures, facilitating beamforming design and power allocation [6]. Compared to reflective RISs, transmissive RISs boast higher aperture efficiency due to their structural features, which eliminates the issues of feed source occlusion and the interference from reflected waves [7].

As a primary function of a passive array, beam synthesis (allocation) characterizes the process through which RISs convert the energy from incident electromagnetic waves into reflected or refracted waves, explicitly forming directional beams [8]. In both reflective RIS and transmissive RIS, the beam synthesis functionality can be achieved through phase configuration, and the existing phase configuration methods employed in reflective RIS can be readily applied to transmissive RIS systems due to the similarity of mathematical models [2].

The simple beam scanning can be realized through phase compensations [2], [9], alongside employing exhaustive search techniques [10], hierarchical search methods [11], and machine learning approaches [12] to tackle beam training and alignment. Additionally, certain multi-beam synthesis can be achieved through physical-related transfer functions [13], pattern approximations and lookup table [14], and the superposition of reflection coefficients [15]. Our previous research has also illustrated that by resolving max-min optimization problems, specific beam synthesis capabilities can be attained [8].

However, these studies primarily concentrate on the main beam, with limited consideration for sidelobe energy. Conversely, sidelobes introduce interference and noise, potentially degrading system performance in dense networks or complex environments. Furthermore, the presence of extra sidelobes heightens the risk of information leakage in communications.

In this work, we explore the beam synthesis while incorporating sidelobe constraints. By formulating and optimizing constrained Max-min problems, the proposed framework allows the signal to be either enhanced or physically suppressed in desired spatial directions, manifesting **high-directional beams** or **beam nulls**. To our knowledge, this marks the first successful implementation of flexible beam synthesis and suppression using a passive reconfigurable array.

The main contributions can be summarized as follows:

This work is supported in part by the National Natural Science Foundation of China (NSFC) under Grants NO.12141107 and NO.11801200, and the Interdisciplinary Research Program of HUST (2023JCYJ012).

- **Physical model and constrained Max-min problem formulation.** We present practical and realistic models grounded in geometrical optics to characterize the input/output behaviors of transmissive RISs. Based on that, a max-min optimization problem with non-linear constraints is then formulated to explore the beam synthesis capabilities of the transmissive RIS.
- **Novel methods for constrained Max-min problem.** In this context, we introduce an auxiliary variable, along with a smooth approximation function given by Moreau envelope to reformulate the original constrained Max-min problem, and then iteratively obtain the optimal solution with a bisection-based (BIS) method. In each iteration, a smooth unconstrained sub-problem is solved using an accelerated gradient descent algorithm.
- **Flexible beam synthesis exploration and achievement.** The proposed algorithms enable either precise signal enhancement or suppression across different directions simultaneously. These beam capabilities is applicable to reflective RISs through appropriate modeling and reflection coefficients. Extensive simulations validated the effectiveness of the framework.

## II. SYSTEM MODEL AND PROBLEM FORMULATION

Due to its unique structural characteristics, the transmissive RIS is not only utilized as a relay repeater to establish additional refractive links but is also frequently employed in transceiver architectures, as illustrated in Fig. 1. In this section, we consider a transmissive RIS-assisted multi-user downlink system including both of the scenarios, with the distinction being the distance from the incident sources to the RIS<sup>1</sup>. We suppose the presence of unauthorized users such as eavesdroppers or users from a neighboring cell.

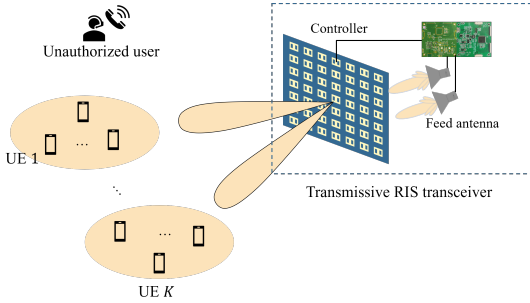


Fig. 1. The communication system involving a transceiver architecture using transmissive RIS.

### A. System Model

We concentrate on an arbitrary transmissive RIS situated on the  $xoy$ -plane, with its geometric center located at the origin of the coordinate system, as shown in Fig. 2. The RIS is a uniformly array consisting of  $N$  units located at  $\mathbf{p}_n = [x_n, y_n, z_n]^T$ ,  $n = 1, \dots, N$ . The unit spacing along

<sup>1</sup>It is reasonable as we focus on radiated waves and do not consider the situation that RIS situated in the reactive near-field region of sources [16].

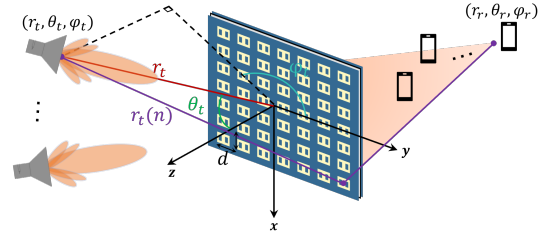


Fig. 2. System model of transmissive RIS-assisted communications.

both the  $x$  axis and  $y$  axis is  $d$ , typically half the wavelength. Assume the RIS is illuminated by a single incident EM wave with electric field  $E^i(r_t, \theta_t, \phi_t)$ , originating from the source point  $(r_t, \theta_t, \phi_t)$ , where  $r_t$ ,  $\theta_t$ , and  $\phi_t$  denote the distance, the elevation angle, and the azimuth angle.

As the EM wave propagates towards the  $n$ -th unit, the attenuation behavior is characterized by the factor  $e^{-j2\pi r_t(n)/\lambda}/r_t(n)$ . Considering the unit on the RIS is isotropic, with scattering pattern  $g$ , the scattered field at the unit can be expressed as  $E^i e^{-j2\pi r_t(n)/\lambda}/r_t(n) g e^{\Omega_n}$ . Similarly, involves propagation towards the UE, the electric field at the observation point along the  $n$ -th unit can be expressed as

$$E^s(n)(r_r, \theta_r, \phi_r) = g e^{\Omega_n} \frac{e^{-j2\pi r_t(n)/\lambda} e^{-j2\pi r_r(n)/\lambda}}{r_t(n)r_r(n)} E^i(r_t, \theta_t, \phi_t), \quad (1)$$

where  $\lambda$  denotes the wavelength,  $r_t(n)$  and  $r_r(n)$  represents the distance from the  $n$ -th unit of the RIS to the transmitter (Tx) and the receiver (Rx), and  $\Omega_n$  represents the phase configuration of the  $n$ -th unit<sup>2</sup>. Thus, the electric field at the observation point is determined by the superposition of individual fields scattered by  $N$  units, given by  $E^s(r_r, \theta_r, \phi_r) = \sum_n g e^{\Omega_n} \frac{e^{-j2\pi r_t(n)/\lambda} e^{-j2\pi r_r(n)/\lambda}}{r_t(n)r_r(n)} E^i(r_t, \theta_t, \phi_t)$ .

Suppose that the illumination signals originate from multiple directions with strengths denoted by  $\{E^i(r_m^t, \theta_m^t, \phi_m^t), m = 1, \dots, M\}$ <sup>3</sup>, the observed electric field is the superposition of multiple electric fields, as

$$E^s(r_r, \theta_r, \phi_r) = \sum_{m=1}^M E^i(r_m^t, \theta_m^t, \phi_m^t) \sum_{n=1}^N g e^{j\Omega_n} \frac{e^{-j2\pi r_m^t(n)/\lambda} e^{-j2\pi r_r(n)/\lambda}}{r_m^t(n)r_r(n)}. \quad (2)$$

Furthermore, if there are  $K$  observation UE points in the far field, the observed electric field at different UE points can be expressed as in (3). Here,  $E^s(r_k^r, \theta_k^r, \phi_k^r)$  denotes the field at UE  $k$ . The terms  $\theta_m^t(n)$ ,  $\phi_m^t(n)$  denote the elevation angle and azimuth angle of the  $m$ -th incident EM wave relative to the  $n$ -th unit. The direction vector is defined as  $\mathbf{u}(\theta, \phi) = [\sin \theta \cos \phi, \sin \theta \sin \phi, \cos \theta]^T$ . The advantage of the canonical linear representation (3) is that it identifies

<sup>2</sup>Here we consider only the phase shifts introduced by the RIS units, assuming the amplitude remains constant.

<sup>3</sup> $\theta_r$  usually falls within the range  $(90^\circ, 180^\circ]$  while  $\theta_t \in [0^\circ, 90^\circ)$ .

$$\begin{aligned}
\begin{bmatrix} E^s(r_1^r, \theta_1^r, \phi_1^r) \\ \vdots \\ E^s(r_K^r, \theta_K^r, \phi_K^r) \end{bmatrix} &\approx g \begin{bmatrix} \frac{e^{-j2\pi r_1^r/\lambda}}{r_1^r} & & 0 \\ & \ddots & \\ 0 & & \frac{e^{-j2\pi r_K^r/\lambda}}{r_K^r} \end{bmatrix} \begin{bmatrix} e^{j2\pi \mathbf{p}_1^T \mathbf{u}(\theta_1^r, \phi_1^r)/\lambda} & \dots & e^{j2\pi \mathbf{p}_N^T \mathbf{u}(\theta_1^r, \phi_1^r)/\lambda} \\ \vdots & \ddots & \vdots \\ e^{j2\pi \mathbf{p}_1^T \mathbf{u}(\theta_K^r, \phi_K^r)/\lambda} & \dots & e^{j2\pi \mathbf{p}_N^T \mathbf{u}(\theta_K^r, \phi_K^r)/\lambda} \end{bmatrix} \begin{bmatrix} e^{j\Omega_1} & & 0 \\ & \ddots & \\ 0 & & e^{j\Omega_N} \end{bmatrix} \\
&\begin{bmatrix} e^{j2\pi \mathbf{p}_1^T \mathbf{u}(\theta_1^i(1), \phi_1^i(1))/\lambda} & \dots & e^{j2\pi \mathbf{p}_1^T \mathbf{u}(\theta_M^i(1), \phi_M^i(1))/\lambda} \\ \vdots & \ddots & \vdots \\ e^{j2\pi \mathbf{p}_N^T \mathbf{u}(\theta_1^i(N), \phi_1^i(N))/\lambda} & \dots & e^{j2\pi \mathbf{p}_N^T \mathbf{u}(\theta_M^i(N), \phi_M^i(N))/\lambda} \end{bmatrix} \begin{bmatrix} \frac{e^{-j2\pi r_1^i/\lambda}}{r_1^i} & & 0 \\ & \ddots & \\ 0 & & \frac{e^{-j2\pi r_M^i/\lambda}}{r_M^i} \end{bmatrix} \begin{bmatrix} E(r_1^i, \theta_1^i, \phi_1^i) \\ \vdots \\ E(r_M^i, \theta_M^i, \phi_M^i) \end{bmatrix}. \quad (3)
\end{aligned}$$

the inherent structure within the channel, capturing the phase variations and radial attenuation resulting from different paths.

### B. Problem Formulation

Considering the presence of unauthorized users in addition to target UEs, we explore a beam synthesis strategy aimed at maximizing the minimum power of UEs, while imposing constraints to ensure that power at undesired positions remains below a predefined threshold. This approach is not only for enhanced signal at target UEs but also provides a solution for addressing information leakage and interference with other users. Formally, this synthesis strategy can be expressed as

$$\begin{aligned}
&\max_{\Omega_1, \dots, \Omega_N \in [0, 2\pi]} \min_k \{P^s(r_k^r, \theta_k^r, \phi_k^r), k = 1, \dots, K\} \\
&\text{s.t. } P^s(r_q^r, \theta_q^r, \phi_q^r) \leq \sigma_q, q = K + 1, \dots, K + Q. \quad (4)
\end{aligned}$$

In this context, we consider  $K$  served UEs and  $Q$  illegitimate users, the notation  $P^s(\cdot) = |E^s(\cdot)|^2$  represents the power at a specific location, and  $\sigma_q$  is the threshold value.

With the input/output models (2) and (3), we can derive representations of the received power under different scenarios. By leveraging them and defining

$$\begin{aligned}
h_n(r_r, \theta_r, \phi_r) &= g \sum_{m=1}^M \frac{E^i(r_m^t, \theta_m^t, \phi_m^t) e^{-j2\pi r_m^t/\lambda} e^{-j2\pi r_r/\lambda}}{r_m^t r_r} \\
&e^{j2\pi \mathbf{p}_1^T \mathbf{u}(\theta^r, \phi^r)/\lambda} e^{j2\pi \mathbf{p}_n^T \mathbf{u}(\theta_m^i(n), \phi_m^i(n))/\lambda} \quad (5)
\end{aligned}$$

The received power can be expressed as

$$P^s(r_r, \theta_r, \phi_r) \approx \left| \sum_{n=1}^N e^{j\Omega_n} h_n(r_r, \theta_r, \phi_r) \right|^2 \quad (6)$$

Introducing  $\mathbf{h} = [h_1(r_r, \theta_r, \phi_r), \dots, h_N(r_r, \theta_r, \phi_r)]^T$ , and  $\mathbf{w} = [e^{j\Omega_1}, \dots, e^{j\Omega_N}]^H$ , the received power at position  $(r_r, \theta_r, \phi_r)$  can be further rewritten as

$$P^s(r_r, \theta_r, \phi_r) \approx \mathbf{w}^H \mathbf{H} \mathbf{w}, \quad (7)$$

where  $\mathbf{H} = \mathbf{h} \mathbf{h}^H$  is a non-negative semi-definite Hermitian matrix. Thus, we can rewrite the problem in (4) as

$$\begin{aligned}
&\max_{\Omega_1, \dots, \Omega_N \in [0, 2\pi]} \min_{1 \leq k \leq K} \mathbf{w}^H \mathbf{H}_k \mathbf{w} \\
&\text{s.t. } \mathbf{w}^H \mathbf{H}_q \mathbf{w} \leq \sigma_q, q = K + 1, \dots, K + Q. \quad (8)
\end{aligned}$$

Furthermore, we can introduce weighting factors  $\alpha_k$  to control signal power among different served UE directions [8]. For clarity, we define a matrix  $\mathbf{A}_k \in \mathbb{C}^{N \times N}$  to incorporate the factor as  $\mathbf{A}_k = 1/\alpha_k \mathbf{H}_k$ . Finally, the optimization problem to achieve beam synthesis can be formulated as

$$\begin{aligned}
(\text{P0}) \quad &\max_{\Omega_1, \dots, \Omega_N \in [0, 2\pi]} \min_{1 \leq k \leq K} \mathbf{w}^H \mathbf{A}_k \mathbf{w} \\
&\text{s.t. } \mathbf{w}^H \mathbf{H}_q \mathbf{w} \leq \sigma_q, q = K + 1, \dots, K + Q. \quad (9)
\end{aligned}$$

It is important to note that besides the optical model above, the problems involving quadratic forms frequently emerge in reflective RISs scenarios and other research domains [17]. We will develop methods that effectively address these issues in the following Section. We emphasize once more that  $\mathbf{w}$  resides in the union of tori<sup>4</sup>, a highly non-convex set, rather than the Hilbert space  $\mathbb{C}^N$ . We also note that the domain of  $\Omega_n$  ( $n = 1, \dots, N$ ) can be relaxed to  $\mathbb{R}$  for periodicity.

### III. OPTIMIZATION METHOD FOR THE CONSTRAINED MAX-MIN PROBLEM.

Problem (P0) belongs to a class of semi-infinite Max-min problems with non-convex constraints. In what follows, we denote  $\boldsymbol{\Omega} = (\Omega_1, \dots, \Omega_N) \in \mathbb{R}^N$  for the sake of simplicity. Recall that  $\mathbf{w} = [e^{j\Omega_1}, \dots, e^{j\Omega_N}]^H \in \mathbb{T}^N$  ( $N$ -tori), we define the following functions

$$\begin{cases} f_k(\mathbf{w}) = -\mathbf{w}^H \mathbf{A}_k \mathbf{w}, \text{ where } k = 1, \dots, K, \\ g_q(\mathbf{w}) = \mathbf{w}^H \mathbf{H}_q \mathbf{w}, \text{ where } q = K + 1, \dots, K + Q. \end{cases} \quad (10)$$

Since  $\mathbb{T}^N$  is compact,  $f_k(\mathbf{w})$  is bounded and compact. Then the problem (P0) is equivalent to

$$\begin{aligned}
&\max_{\boldsymbol{\Omega}} \min_{1 \leq k \leq K} -f_k(\mathbf{w}) = -\min_{\boldsymbol{\Omega}} \max_{1 \leq k \leq K} f_k(\mathbf{w}) \\
&\text{s.t. } g_q(\mathbf{w}) \leq \sigma_q, \quad (11)
\end{aligned}$$

where  $f_k(\mathbf{w})$  and  $g_q(\mathbf{w})$  are continuous differentiable with Lipschitz continuous gradient ( $C^{1,1}$  smooth). It is known that projection onto  $\mathbb{R}^N$  is simple. We introduce a variable  $t \in \mathbb{R}$ , and the constraint minimization problem is equivalent to

$$\begin{aligned}
&\min_{\boldsymbol{\Omega}} t \\
&\text{s.t. } f_k(\mathbf{w}) - t \leq 0, g_q(\mathbf{w}) - \sigma_q \leq 0. \quad (12)
\end{aligned}$$

<sup>4</sup>Tori is the direct product of unit circles.

We define the function

$$F(t) = \min_{\Omega} \max \left\{ \{f_k(\mathbf{w}) - t\}_{k=1}^K, \{g_q(\mathbf{w}) - \sigma_q\}_{q=K+1}^{K+Q} \right\}. \quad (13)$$

then the constraint problem (12) is equivalent to solving

$$F(t) = 0$$

The function  $F(t)$  is monotonically decreasing in  $t$ , so that  $F(t) = 0$  has a unique solution. This root can be found by the bisection method (linear convergence), in which the sign of  $F(t)$  is needed in each iteration. Note that evaluating  $F(t)$  is equivalent to solving an unconstrained minimax problem, which can also be regarded as an unconstrained minimization problem with the objective function given by the maximum function composed with differentiable functions. Since (13) is non-smooth due to the presence of the maximum function, we utilize the Moreau envelope of the maximum function, which is a tight smooth approximation. We denote the maximum function by  $M(x)$  for  $x \in \mathbb{R}^{K+Q}$ , then its Moreau envelope  $M_\lambda(x)$  is written as [18]

$$M_\lambda(\mathbf{x}) = \min_{\mathbf{z}} M(\mathbf{z}) + \lambda \|\mathbf{z} - \mathbf{x}\|^2, \quad (14)$$

where  $\lambda$  is the regularization parameter. As calculated in [19], [20],  $M_\lambda(\mathbf{x})$  has explicit form

$$M_\lambda(\mathbf{x}) = \lambda \|\mathbf{x}\|^2 - \frac{1}{4\lambda} \|2\lambda\mathbf{x} - P_\Delta(2\lambda\mathbf{x})\|^2, \quad (15)$$

where  $\Delta = \{\mathbf{x} \in \mathbb{R}_+^{K+Q} : \sum_k x_k \leq 1\}$  is the unit simplex,  $P_\Delta$  is the projection onto  $\Delta$ . The gradient of  $M_\lambda(\mathbf{x})$  is

$$D_x M_\lambda(\mathbf{x}) = P_\Delta(2\lambda\mathbf{x}), \quad (16)$$

which is  $2\lambda$ -Lipschitz continuous. We denote the objective function in (13) by

$$h_{K+Q}(\mathbf{w}, t) = \left\{ \{f_k(\mathbf{w}) - t\}_{k=1}^K, \{g_q(\mathbf{w}) - \sigma_q\}_{q=K+1}^{K+Q} \right\},$$

then  $F(t)$  in (13) is written as

$$F(t) = \min_{\Omega} M(h_{K+Q}(\mathbf{w}, t)),$$

which has an approximation

$$F_\lambda(t) = \min_{\Omega} M_\lambda(h_{K+Q}(\mathbf{w}, t)). \quad (17)$$

Instead of finding the value of  $F(t)$ , we evaluate  $F_\lambda(t)$  by solving the smooth unconstrained optimization problem (17) using gradient-based methods such as Nesterov's accelerated gradient descent method [8], [21], [22]. Additionally,  $F_\lambda(t)$  is also monotonically decreasing in  $t$  and has a root for  $\lambda$  sufficiently large. The error of the approximation is given by [20]

$$-\frac{1}{4\lambda} \leq F_\lambda(t) - F(t) \leq 0, \quad (18)$$

which is independent of the dimension of the problem and serves as the key role in error estimate. The tightness of the approximation is shown by the uniform convergence of the error as  $\lambda \rightarrow \infty$ .

The algorithm for finding the root of  $F$  and the optimum of the original problem (9) is summarized in Algorithm 1. Note that while employing the bisection method to find the root of  $F$ ,  $F_\lambda$  instead of  $F$  is evaluated in each iteration. It is readily checked that if  $F_\lambda(t) > 0$ , then  $F(t) > 0$ ; if  $F_\lambda(t) < -\frac{1}{4\lambda}$ , then  $F(t) < 0$ . The number of iterations is at most  $\lceil \log_2 \delta \rceil$ . The computational complexity for evaluating  $F_\lambda(t)$  is  $\mathcal{O}(N)$ , where  $N$  represents the size of the search space. As the algorithm concludes, the returned value  $t^*$  satisfies  $|F(t^*)| < \delta$ , and corresponding  $\Omega^*$  achieves the optimal objective of the original problem (9) within at most  $\delta$  while the constraints are satisfied within a tolerance of at most  $\delta$ .

---

**Algorithm 1** Bisection-based method (BIS) for constrained Max-min problem (9)

---

**Input:**  $\mathbf{A}_k, \mathbf{H}_q$ , the threshold  $\sigma_q$ , initial parameter  $\lambda_0$ , tolerance  $\epsilon, \delta$ .

**Output:** Optimum  $\Omega^*$ , the root  $t$

- 1: Construct  $F_\lambda(t)$  and initialize  $a, b$ , such that  $F_\lambda(a) > 0$  and  $F_\lambda(b) < -\frac{1}{4\lambda}$ .
  - 2:  $\lambda \leftarrow \lambda_0$ ;
  - 3: **while**  $|a - b| > \epsilon$  **do**
  - 4:    $t \leftarrow a + \frac{b-a}{2}$
  - 5:   Solve (17) for optimum  $\Omega^*$  and evaluate  $F_\lambda(t)$ ;
  - 6:   **if**  $F_\lambda(t) < -\frac{1}{4\lambda}$  **then**
  - 7:      $b \leftarrow t$ ;
  - 8:   **else if**  $F_\lambda(t) > 0$  **then**
  - 9:      $a \leftarrow t$ ;
  - 10:   **else if**  $\lambda > \frac{1}{4\delta}$  **then**
  - 11:     **return** ;
  - 12:   **else**
  - 13:      $\lambda \leftarrow 2\lambda$ ;
  - 14:   **end if**
  - 15: **end while**
  - 16: **return**  $\Omega^*, t$
- 

#### IV. NUMERICAL SIMULATION EVALUATIONS

We now investigate the effectiveness of the proposed framework<sup>5</sup>. Initially, we evaluate the beam suppression and the flexible multi-beam synthesis. Subsequently, we analyze the impact of the constraint threshold on beam performance and compare the proposed method with two established algorithms, including SDR-SDP [23] and QuantRand [24]. Additionally, we consider the sidelobe-unconstrained scheme, which solves the problem (P0) without its constraint using the latest MA algorithm [8] as a benchmark, denoted as 'Non-constraint'.

The SDR-SDP method is based on semi-definite relaxation and semi-definite programming techniques, while QuantRand is a quantized version of random coordinate descent, employing a greedy algorithm. The employed transmissive RIS operates at a frequency of 5.8 GHz. In all trials, the transmitting power at each source is set to 0 dBm, and the distances from the UE to the RIS are fixed at 30 m.

<sup>5</sup>The results can be reproduced using codes available at: [https://github.com/RujingXiong/RIS\\_BeamAllocation](https://github.com/RujingXiong/RIS_BeamAllocation).

### A. Beam Synthesis and Suppression

1) *Directional Suppression*: We begin by evaluating the suppression performance using a linear transmissive RIS composed of 16 units. We consider an incident signal original from (5 m,  $0^\circ, 0^\circ$ ) and two targets UEs at directions ( $160^\circ, 180^\circ$ ) and ( $150^\circ, 0^\circ$ ) (corresponding observation angles  $-20^\circ$  and  $30^\circ$ ) with equal weight. Assuming that the unauthorized users are located within the range of  $-10^\circ$  to  $0^\circ$ . The cross-sections of the beams at distance  $r_r = 30$  m, as a function of the observation angle  $\theta$ , are shown in Fig. 3(a). It is evident that, in addition to forming high directional beams at the UE directions, the signal energy within the region from  $-10^\circ$  to  $0^\circ$  is completely suppressed, resulting a distinct beam null.

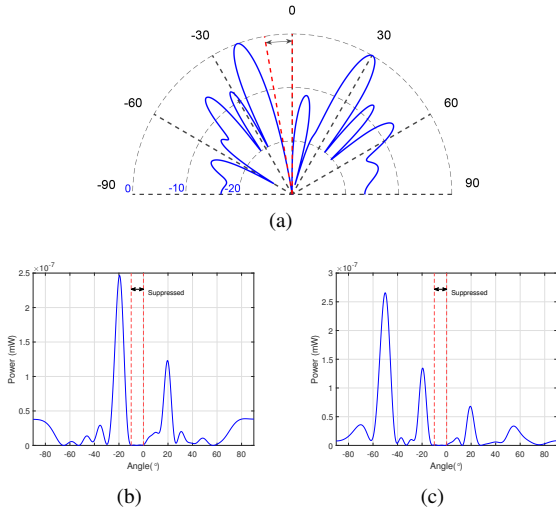


Fig. 3. Beam synthesis with the suppression interval bounded by two red dashed lines is  $[-10^\circ, 0^\circ]$ . (a) UE 1 and UE 2 are set with equal weight. (b) UE 1 and UE 2 are set with weight factors  $\alpha_1 = 2, \alpha_2 = 1$ . (c) Three UEs are set with  $\alpha_1 = 4, \alpha_2 = 2, \alpha_3 = 1$ .

2) *Flexible Beam Allocation*: The beam synthesis capability is further evaluated while maintaining the suppression. By adjusting the weight for each target UE, we can realize flexible beam control across various directions. As demonstrated in Fig. 3(b) and Fig. 3(c), while keeping a beam null from  $-10^\circ$  to  $0^\circ$ , we successfully achieved beam energy allocation in ratio of 2:1 for two, and of 4:2:1 for three different UE directions. This functionality allows us to freely achieve spatial energy distribution when utilizing transmissive RIS for beam synthesis, whether in signal enhancement or suppression.

### B. Beam Comparison and Evaluation

To assess the beam synthesis performance of the proposed algorithm, we compare it against existing methods. In this test, the suppressed region is from  $-36^\circ$  to  $-20^\circ$ , and equal weight factor for the two served UEs at  $20^\circ$  and  $50^\circ$  are configured. We present the radiation patterns in Fig. 4. It can be observed that the proposed BIS algorithm achieves effective energy suppression in the target region while maintaining a main beam power level comparable to the Non-constraint baseline. In contrast, the SDR-SDP method delivers such poor

suppressions that are even worse than the unconstrained case. Furthermore, while the QuantRand algorithm exhibits commendable suppression performance to some extent, its limited energy performance in the two main beams (UEs) indicates that it is not a reasonable solution. For comprehensive, we vary the weight factors and repeat the trials, with the results and performance metrics associated with various algorithms summarized in Table I. It can be observed that the proposed algorithm simultaneously achieves both the precise main beam power level control and effective sidelobe beam suppression, which existing works cannot accomplish.

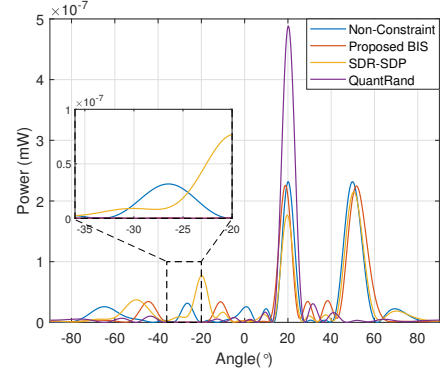


Fig. 4. Beam pattern comparison of various methods. The suppressed region is set to  $[-36^\circ, -20^\circ]$ .

TABLE I  
METRICS COMPARISONS, THE SUPPRESSED ANGLE INTERVAL IS ( $\theta_{SUP} = [-36^\circ, -20^\circ]$ )

Weight	Methods	Actual power	Variance	Peak of Sup
1 : 1	Non-Constraint	1:1	0	-75.01 dBm
	<b>Proposed BIS</b>	<b>1:1</b>	<b>0</b>	<b>-93.77</b> dBm
	QuantRand	217:1	23328	-92.91 dBm
	SDR-SDP	0.822:1	0.016	-71.14 dBm
1 : 2	Non-Constraint	1:2	0	-75.63 dBm
	<b>Proposed BIS</b>	<b>1:2</b>	<b>0</b>	<b>-94.62</b> dBm
	QuantRand	164:2	13278	-92.43 dBm
	SDR-SDP	1:2.19	0.0181	-72.82 dBm

### C. Analysis of the Relative Power Gain

For a clearer demonstration of the beam synthesis gains provided by the proposed methods, we analyze the received signal power at the target UEs and the suppression points and define the metric of relative gain (RG), calculated by

$$RG = 10 \log_{10}(P_{UE,min}/P_{SP,max}),$$

where  $P_{UE,min}$  measures the minimum power level within the served UEs, and  $P_{SP,max}$  accounts for the maximum within suppressed positions. We conduct two tests, the first focuses on the impacts of the number of RIS units  $N$  on RG performance, while the second examines the influence of the number of

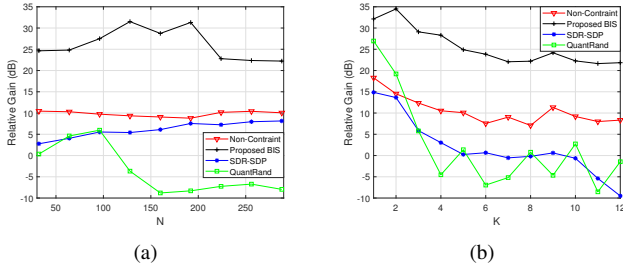


Fig. 5. Comparison of RG performance with equal-weight UEs. (a) As a function of the number of RIS units, with three UEs at  $(110^\circ, 20^\circ)$ ,  $(140^\circ, 0^\circ)$ , and  $(140^\circ, 180^\circ)$ . (b) As a function of the number of UEs, the number of RIS units  $N = 16$ .

served UEs  $K$ . The suppressed region is set to  $[-36^\circ, -20^\circ]$ . To ensure robustness, we conduct 100 trials for each value of  $N$  or  $K$  and calculate the average values.

The results plotted in Fig. 5(a) indicate that, the RG performance of the Non-constraint scheme stabilizes around 10 dB with an increase in the number of units. This suggests that although the received power will increase with the number of RIS units [17], the sidelobe energy also rises, maintaining a nearly constant ratio between the two. In other words, in practical applications, employing a larger RIS to serve users will inevitably heighten the risk of interference or information leakage in sidelobe directions.

As we focus on sidelobe suppressing, we observe that methods such as SDR-SDP and QuantRand exhibit even poorer RG performance than Non-constraint. When the number of units exceeds 120, the RG achieved by QuantRand falls below zero, demonstrating that the beam energy directed towards undesired directions surpasses that of the target communication UEs. In contrast, the proposed BIS achieves an RG of up to 25 dB. This significant difference between the main beam and the sidelobe power level ensures its capability to prevent signal interference and information leakage. The same trend is observed when varying the number of UEs  $K$ , as illustrated in Fig. 5(b), where the proposed method significantly surpasses the competitors.

## V. CONCLUSION

This paper has presented a comprehensive framework for beam synthesis and suppression using transmissive RIS, addressing constrained Max-min optimization problems. In this context, We developed realistic geometrical optics-based models and introduced a novel BIS algorithm capable of solving a broad range of constrained Max-min problems. The proposed framework enables flexible beam allocation, allowing for the enhancement or suppression of beams in specific spatial directions. Simulations have demonstrated the effectiveness of the proposed method, highlighting its superior performance compared to existing algorithms. The proposed method holds great potential for future applications, including, anti-eavesdropping, interference mitigation, multi-target detection and tracking, and energy-efficient networks.

- [1] Q. Wu *et al.*, "Intelligent surfaces empowered wireless network: Recent advances and the road to 6G," *Proc. IEEE*, Jun. 2024, Early access, doi: 10.1109/JPROC.2024.3397910.
- [2] J. Tang *et al.*, "Transmissive ris for B5G communications: Design, prototyping, and experimental demonstrations," *IEEE Trans. Commun.*, vol. 71, no. 11, pp. 6605–6615, Nov. 2023.
- [3] Y. Wang *et al.*, "Doppler shift and channel estimation for intelligent transparent surface assisted communication systems on high-speed railways," *IEEE Trans. Commun.*, vol. 71, no. 7, pp. 4204–4215, Jul. 2023.
- [4] N. Docomo, "DOCOMO conducts world's first successful trial of transparent dynamic metasurface," Jan. 2020, Accessed: 2024-10-04. [Online]. Available: [https://www.docomo.ne.jp/english/info/media\\_center/pr/2020/0117\\_00.html](https://www.docomo.ne.jp/english/info/media_center/pr/2020/0117_00.html)
- [5] J. Zhang *et al.*, "Design and prototyping of transmissive RIS-aided wireless communication," Feb. 2024. [Online]. Available: <https://arxiv.org/abs/2402.05570>
- [6] Z. Li *et al.*, "Beamforming design and power allocation for transmissive RMS-based transmitter architectures," *IEEE Wirel. Commun. Lett.*, vol. 11, no. 1, pp. 53–57, Jan. 2021.
- [7] Z. Liu *et al.*, "Transmissive reconfigurable intelligent surface transmitter empowered cognitive RSMA networks," *IEEE Communications Letters*, vol. 27, no. 7, pp. 1829–1833, Jul. 2023.
- [8] R. Xiong *et al.*, "Fair beam allocations through reconfigurable intelligent surfaces," *IEEE J. Sel. Areas Commun.*, vol. 42, no. 11, pp. 3095–3109, Nov. 2024.
- [9] Y. Han *et al.*, "Cooperative double-IRS aided communication: Beamforming design and power scaling," *IEEE Wirel. Commun. Lett.*, vol. 9, no. 8, pp. 1206–1210, Aug. 2020.
- [10] P. Wang *et al.*, "Beam training and alignment for RIS-assisted millimeter-wave systems: State of the art and beyond," *IEEE Wirel. Commun.*, vol. 29, no. 6, pp. 64–71, Dec 2022.
- [11] J. Wang *et al.*, "Hierarchical codebook-based beam training for RIS-assisted mmwave communication systems," *IEEE Trans. Commun.*, vol. 71, no. 6, pp. 3650–3662, Jun. 2023.
- [12] Y. Heng *et al.*, "Machine learning-assisted beam alignment for mmwave systems," *IEEE Trans. Cogn. Commun. Netw.*, vol. 7, no. 4, pp. 1142–1155, Dec. 2021.
- [13] S. Droulias *et al.*, "Reconfigurable intelligent surfaces as spatial filters," *IEEE Trans. Wirel. Commun.*, Aug. 2024, early access, doi: 10.1109/TWC.2024.3447910.
- [14] M. Rahal *et al.*, "Performance of RIS-aided near-field localization under beams approximation from real hardware characterization," *EURASIP J. Wirel. Commun. Netw.*, vol. 2023, no. 1, p. 86, Aug. 2023.
- [15] S. Meng *et al.*, "An efficient multi-beam generation method for millimeter-wave reconfigurable intelligent surface: Simulation and measurement," *IEEE Trans. Veh. Technol.*, vol. 72, no. 10, pp. 13 752–13 757, Oct. 2023.
- [16] Y. Liu *et al.*, "Near-field communications: A tutorial review," *IEEE Open J. Commun. Soc.*, vol. 4, pp. 1999–2049, Aug. 2023.
- [17] R. Xiong *et al.*, "Optimal discrete beamforming of RIS-aided wireless communications: An inner product maximization approach," 2024. [Online]. Available: <https://arxiv.org/abs/2211.04167v6>
- [18] J.-J. Moreau, "Proximité et dualité dans un espace hilbertien," *Bulletin de la Société mathématique de France*, vol. 93, pp. 273–299, 1965.
- [19] K. Zhang, "Compensated convexity and its applications," *Ann. Inst. Henri Poincaré-Anal. Non Linéaire*, vol. 25, no. 4, pp. 743–771, Jan. 2008.
- [20] K. Yin *et al.*, "A tight smooth approximation of the maximum function and its applications," *J. Convex Anal.*, vol. 29, no. 4, pp. 1193–1224, Apr. 2022.
- [21] Y. Nesterov, "Introductory lectures on convex programming volume i: Basic course," *Lect. Notes*, vol. 3, no. 4, p. 5, Jul. 1998.
- [22] O. Devolder *et al.*, "First-order methods of smooth convex optimization with inexact oracle," *Math. Program.*, vol. 146, no. 1-2, pp. 37–75, Aug. 2014.
- [23] H. Li, H. Wang, and P. Li, "Weighted sum-rate maximization for collaborative-RIS-assisted downlink MISO system," *IEEE Wirel. Commun. Lett.*, vol. 13, no. 6, pp. 1740–1744, Jun. 2024.
- [24] A. Subhash *et al.*, "Max-Min SINR optimization for RIS-aided uplink communications with green constraints," *IEEE Wirel. Commun. Lett.*, vol. 12, no. 6, pp. 942–946, Jun. 2023.